Wind Turbine Diffuser Aerodynamic Study with OpenFOAM®

Félix Sorribes-Palmer, Antonio Figueroa-González, Ángel Sanz-Andrés and Santiago Pindado

Abstract The aim of this work is to analyze the influence of the pressure losses of a diffuser-augmented wind turbine (DAWT) on the extractable power. Multielement diffuser geometries, generated with Salome and meshed with snappyHexMesh, are studied numerically with OpenFOAM® to find a configuration of maximum area expansion (reducing flow detachment), for different pressure losses at the actuator disk. Different geometries are studied with a $k-\varepsilon$ turbulence model. The influence of the vanes inside the diffuser has also been analyzed. The results of the present work show the importance of a careful design of the diffuser entrance.

AQ1

1 Introduction

The extractable energy of a horizontal axis turbine rotor of fixed size can be increased by installing it at the entrance of a diffuser. The flow around flange diffusers has been studied experimentally and numerically by many researchers [1, 3, 10]. By recovering exhaust kinetic energy, the diffuser produces a greatly reduced pressure behind the turbine compared to the one behind a bare turbine. This effect increases the mass flow rate through the DAWT, with at least as much pressure change as across a conventional turbine [5]. The overall effect is to increase the power produced for a given rotor diameter. The increase of the mass flow rate in the diffuser is influenced by four main factors [11]:

- The diffuser area ratio A_{ex}/A_c.
- The flow separation downstream in the diffuser.
- The base pressure reduction at the diffuser exit caused by the obstruction flow.
- Viscous losses.

According to Blevins' Handboook [2], the flow separation in a diffuser, also called the diffuser stall, depends on diffuser inlet and outlet conditions, Reynolds number,

F. Sorribes-Palmer (✉) · A. Figueroa-González · Á. Sanz-Andrés · S. Pindado
Instituto Universitario de Microgravedad Ignacio Da Riva, Universidad Politécnica de Madrid, Madrid, Spain
e-mail: felix.sorribes@upm.es

J. M. Nóbrega and H. Jasak (eds.), *OpenFOAM®*,
https://doi.org/10.1007/978-3-319-60846-4_37

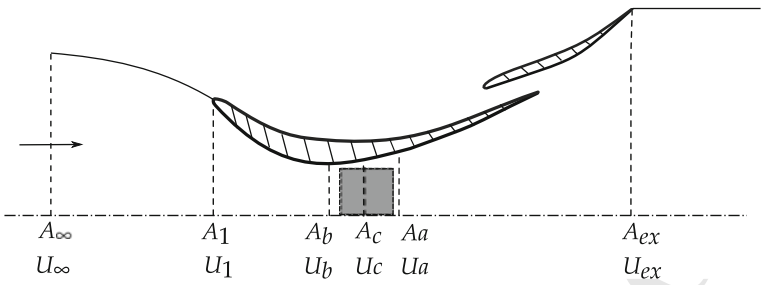

Fig. 1 Sketch of a general DAWT duct. The areas and flow velocities at the characteristic section of the duct are indicated

Mach number, and diffuser geometry. In the aforementioned handbook, diffuser stall is studied for different configurations: two-dimensional, conical, annular, straight-walled, and curved wall diffusers. It also includes an analysis of the influence of different diffuser geometry parameters on different stall regimes: first appreciable, large transitory, fully developed, hysteresis zone, and jet flow.

A general schema of a DAWT duct is shown in Fig. 1. In this work, a configuration with two slots in the diffuser is analyzed as an improvement, bearing in mind that the tangential injection of air available from the external wind supplied to the boundary layer helps the main flow overcome the adverse pressure gradient and frictional losses in the wall region. Additionally, the effect of a vane installed in the duct was analyzed too. Vanes subdivide the diffuser into a series of diffusing passages, each of which will have divergence angles and area ratios much smaller than those of the vaneless diffuser [2].

The sampled sections are far field upstream A_∞, the inlet A_1, the section immediately upstream of the turbine A_b, the turbine section A_c, the section immediately downstream of the turbine A_a and the diffuser exit A_{ex}.

The present work is organized as follows: in Sect. 2, the main parameters of DAWT performance are presented. In Sect. 3, the CFD numerical set up of different configurations for finding the maximum extractable power are summarized, whereas the main results of the simulations are described in Sect. 4. Finally, in Sect. 5, the main conclusions of the numerical study is drawn.

2 Analytical Framework

The different cases are compared by analyzing the variation of pressure through the duct; from the energy conservation equation, for a steady and incompressible flow [8], the relation between the exit and freestream condition is given by

$$p_\infty + \frac{1}{2}\rho U_\infty^2 = p_{ex} + \frac{1}{2}\rho U_{ex}^2 + \Delta p_c + \Delta p_d\,, \tag{1}$$

where ρ is the density of the fluid, p_∞ is the pressure far upstream, p_{ex} is the pressure at the diffuser exit, Δp_c and Δp_d are the total pressure losses in the turbine and in the duct, respectively, and U_∞ and U_{ex} are the flow speed upstream and at the exit of the duct (see Fig. 1). The total pressure losses ($\Delta p = \Delta p_c + \Delta p_d$) can be modeled as

$$\Delta p_c = k_{pc}\frac{1}{2}\rho U_c^2\,, \quad \Delta p_d = k_{pd}\frac{1}{2}\rho U_c^2\,. \tag{2}$$

Besides, the pressure loss coefficient in the turbine can be referred to the flow speed upstream U_∞, with the cross section area ratio, $\lambda = A_{ex}/A_c = U_c/U_{ex}$:

$$K_{pc} = \frac{\Delta p_c}{\frac{1}{2}\rho U_c^2}\lambda^2 = k_{pc}\lambda^2\,. \tag{3}$$

From Betz's limit, it can be deduced that the pressure loss at a turbine related to extractable maximum energy is $K_{pc} \sim 2$ [9].

The pressure coefficient at the diffuser exit is

$$c_{pex} = \frac{p_{ex} - p_\infty}{\frac{1}{2}\rho U_\infty^2}\,, \tag{4}$$

where p_∞ and p_{ex} are, respectively, the static pressure of the flow upstream and at the exit.

Finally, the extracted power by the turbine can be estimated as

$$c_{Wc} = \frac{\Delta p_c U_c A_c}{\frac{1}{2}\rho A_c U_\infty^3} = K_{pc}\lambda\left(\frac{U_{ex}}{U_\infty}\right)^3\,. \tag{5}$$

This parameter is used in the present work to compare the different DAWT configurations.

3 Numerical Setup

The open-source CFD software OpenFOAM® has been used to carry out the simulations. The performance analysis of several DAWT duct configurations has been conducted by employing a 2D model, placing a porous region in the throat to simulate an actuator disk.

The length of the studied DAWT duct configurations is about 6 m, with a cross section area ratio $\lambda = 3.7$. The computational domain dimensions are 60 m in length by 24 m in height. The geometries were developed with Salome, through use of

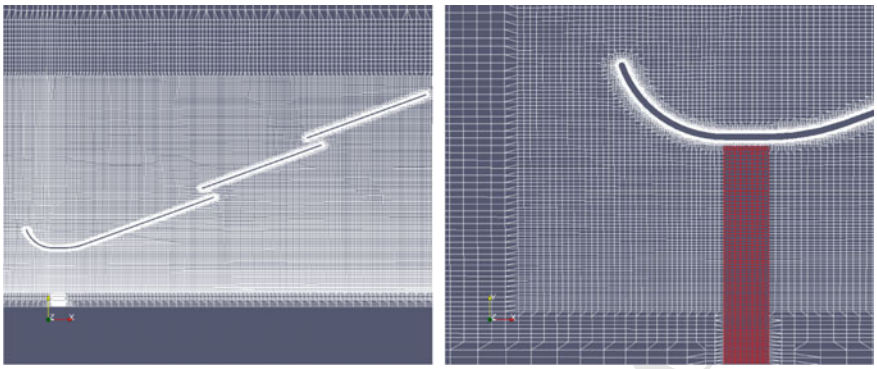

Fig. 2 Mesh details. The porous region is colored in red

a python script, which allowed for the creation of parametric geometries, while the meshes were generated with snappyHexMesh. The procedure followed was to generate the .stl files first, with the mesh subsequently being generated employing surfaceFeatureExtract, snappyHexMesh and extrudeMesh to create the final mesh.

In Fig. 2, one diffuser geometry, together with the detail of the mesh in the porouse region, is shown. The final mesh is obtained from the castellation of the .stl geometries, as indicated in the aforementioned figure. Then, the porosity region was assigned with topoSet using the Darcy–Forchheimer formulation. Only inertial terms, F, were considered to take into account the effect of the porosity in this region. This term was included in the momentum equation as follows [6]:

$$\frac{\partial}{\partial t}(\rho u_i) + u_j \frac{\partial}{\partial x_j}(\rho u_i) = -\frac{\partial p}{\partial x_i} + \mu \frac{\partial \tau_{ij}}{\partial x_j} - \left(\mu D + \frac{1}{2}\rho u_{jj} F\right) u_i \,. \tag{6}$$

Each configuration has been simulated for several values of F. The turbine has been modeled applying the widely known actuator disk theory, placing a thin porous region of 0.2 m in length, in the throat of the turbine. Some examples of the use of porous disks for simulating turbines can be found in [4, 7]. The aforementioned porous region simulates the behavior of the turbine blades: the pressure drops in it, with the obvious advantage of speeding up the numerical simulations. In return, the rotational flow component is lost.

The numerical simulation was performed on the steady RANS equations with a $k - \varepsilon$ turbulence model for computational time reasons, as the main goal of the work is to study the different configurations within a reasonable time. Further work has already been done in [12], in which other turbulence models with and without wall functions have been applied to analyze their influence on the overall performance of DAWT. As it was expected, more complete turbulence models for the analysis of detached flows agree better with the empirical and theoretical relations that describe the evolution of the pressure in DAWTs.

The generated meshes provide y^+ close to 12 in all studied cases. Although y^+ was smaller than 30, wall functions were used to model turbulence at the walls. The Reynolds number based on the length of the first diffuser segment reached up to $Re \sim 550{,}000$, taking a freestream velocity of $U_\infty = 4$ m/s. The turbulence intensity introduced at the inlet was $I_u = 0.03$, the turbulent kinetic energy being calculated as $k = \frac{3}{2}(I_u U_\infty)^{3/2}$, and the dissipation rate as $\varepsilon = \rho C_\mu k/\mu_t$, where $C_\mu = 0.09$ and $\mu_t = 1000 I\mu$. The selection of the turbulence intensity was made based on a previous study in which the diffuser was located in the ground in a fully developed flow using equation $I_u = 0.16 \cdot Re_d^{-1/8}$.

The equations are numerically solved by means of the SIMPLE algorithm, the cell-based solver with the least squares being used. A bounded Gauss linear upwind difference scheme was used for spatial discretization. The solver used was porous-SimpleFoam with moderate underrelaxation factors.

A velocity boundary was used at the inlet and a static pressure boundary was used at the outlet. The top wall was defined as a no-slip boundary, and the back and front as empty so as to simulate a 2D domain. In addition, a symmetry plane boundary

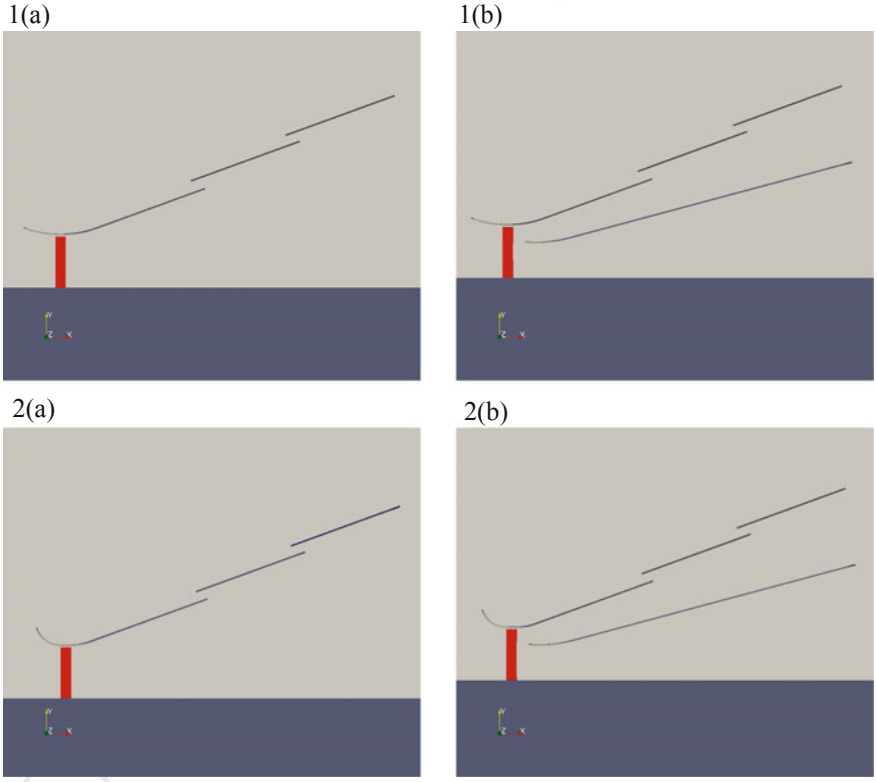

Fig. 3 Diffuser-augmented wind turbine configurations

condition simulating the other half of the turbine is used in the plane $y = 0$. The residuals were monitored using PyFoamPlotRunner, being the convergence criteria to keep the residual values under 10^{-4}. The DAWT duct configurations analyzed are shown in Fig. 3. The red zone represents the porous region simulating the turbine. From configuration (1a) to (1b), an interior vane was introduced to reduce detachment on the diffuser; from (1a) to (2a), the inlet was modified to avoid detachment at the leading edge of the diffuser; finally, between (2a) and (2b), the aforementioned vane has was introduced again.

4 Results

Flow and pressure fields distribution are shown in Figs. 4 and 5 for the different configurations analyzed. In Fig. 5 can be observed how the vanes help to generate a more uniform and negative pressure profile at the exit, a result that can be even better observed in Fig. 6. The suction at the exit induces higher speed and more mass flow rate through the turbine section.

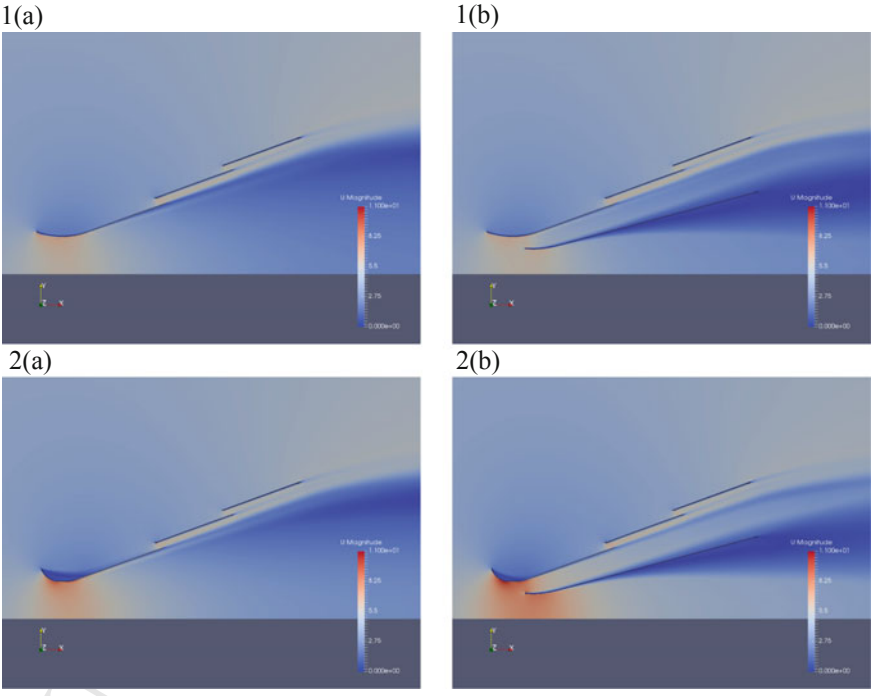

Fig. 4 Velocity fields at the different DAWT configurations for the optimum K_{pc} for each configuration

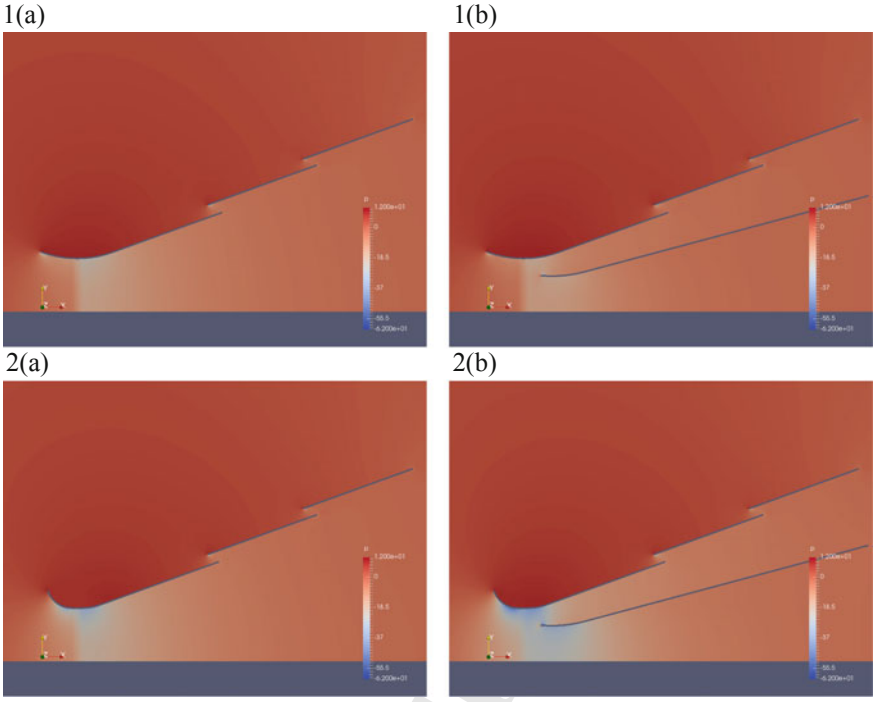

Fig. 5 Pressure fields at the different DAWT configurations for the optimum K_{pc} for each configuration

The profiles of velocity and pressure at the different sections of the DAWT duct configurations are shown in Fig. 6. These graphs indicate that the velocity profile at the first section of the duct is smoother in the configurations with the modified entrance. The flow acceleration in the gap between the porosity region and the diffuser, which helps to maintain the attached boundary layer, can also be observed. At the exit of the ducts, the velocity profile highlights the detached region. While adding a vane barely affects the pressure coefficient at the exit of the DAWT, it is significant that this coefficient decreases when the entrance of the diffuser is modified.

Comparing configurations (1a) and (1b), the effect of the vane implies a reduction of the energy extracted. However, once the entrance was improved [configurations (2a) and (2b)], the vane generated a more negative pressure at the exit, which induces higher speeds. Looking at Eq. 5, for the same pressure drop at the turbine K_{pc}, these higher speeds at the exit increase the energy extracted.

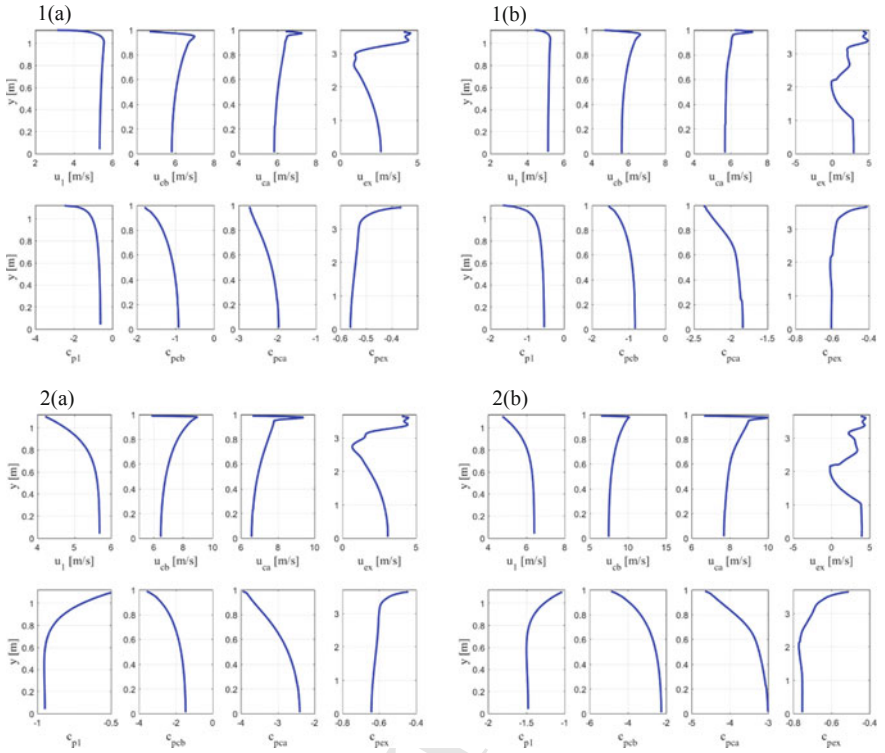

Fig. 6 Velocity and pressure coefficient profiles in the sections A_1, A_{cb}, A_{ca} and A_{ex} for the optimum K_{pc} for each configuration

The curves of the extracted power coefficient and pressure coefficient are shown in Fig. 7. The pressure coefficient has been estimated as an average of the pressure coefficient profile at the exit of the diffuser.

In Table 1, the values of the maximum efficiency in relation to the different DAWT analyzed are summarized. Although the splitter vane helps to reattach the boundary layer at the diffuser, as the flow detaches from the vane, the pressure losses does not compensate, because the configurations with the vane do not improve the performance within the entire simulated range of K_{pc}. A possible solution to this effect could be to split the vane or make it shorter to avoid flow detachment.

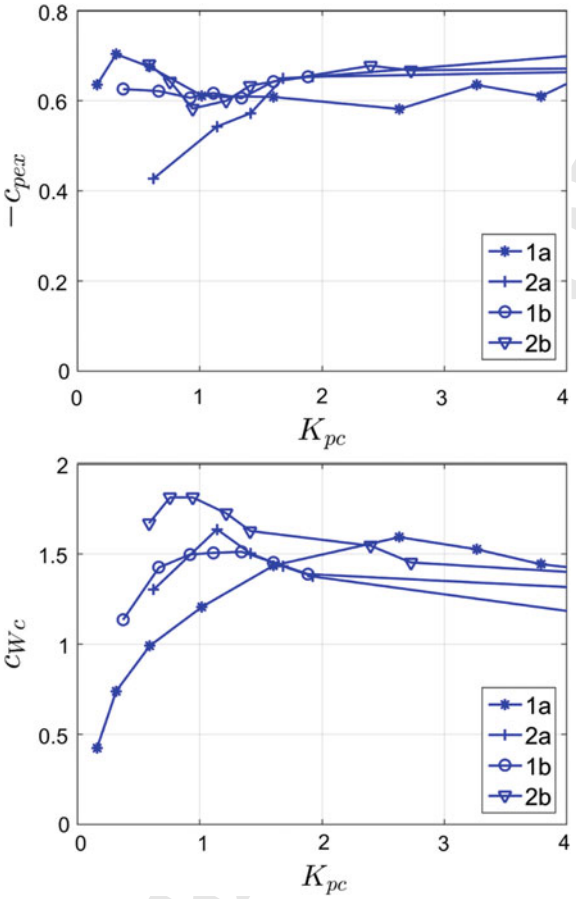

Fig. 7 Pressure coefficient at the turbine exit and specific power extracted

Table 1 Pressure loss coefficient K_{pc} at the for maximum extracted power coefficient C_{Wcmax} for the diffuser configurations

Configuration	N airfoils	K_{pcmax}	C_{Wcmax}
1a	3	2.6	1.6
1b	4	1.3	1.5
2a	3	1.1	1.6
2b	4	0.6	1.8

5 Conclusions

Four different configurations of DAWT ducts have been compared by obtaining the point of maximum extracted energy. The simulations show the importance of a well-designed entrance to the duct, in order to reduce pressure losses due to flow detachment. In addition, when the efficiency entrance increases, the optimum value of the extractable power is obtained for lower values of the coefficient K_{pc}, a result that result agrees with the work of [9]. In comparison with configuration (1a), the flow is detached in (1b) in a part of the vane, causing a reduction of the extractable power. However, when the entrance of the duct is enhanced, installation of a vane increases the extractable energy. Accordingly, the configuration (2b) has the best performance. The obtained value of c_{Wc} exceeds the Betz limit for all configurations.

Acknowledgements The authors thank the OFW11 organizers and to all the contributors who enriched this event. We also want to thank OpenFoamWiki, CFDsupport, Chalmers University, and ICE Stroemungsforschung for their contribution to OpenFoam® documentation.

References

1. Ken Ichi Abe and Yuji Ohya. An investigation of flow fields around flanged diffusers using CFD. *Journal of Wind Engineering and Industrial Aerodynamics*, 92(3–4): 315–330, 2004. ISSN 01676105. https://doi.org/10.1016/j.jweia.2003.12.003.
2. Robert D. Blevins. *Applied Fluid Dynamics Handbook*. New York, 1984. ISBN 9780442212964.
3. Rym Chaker, Mouldi Kardous, Fethi Aloui, and Sassi Ben Nasrallah. Open angle effects on the aerodynamic performances of a flanged Diffuser Augmented Wind Turbine (DAWT). 2014.
4. G. Crasto and A. R. Gravdahl. CFD wake modeling using a porous disc. *European Wind Energy Conference and Exhibition. vol. 6, pp. 3028–3037*, 2008.
5. B.L. Gilbert, R.a. Oman, and K.M. Foreman. Fluid dynamics of diffuser-augmented wind turbines. *Journal of Energy*, 2(6): 368–374, 1978. ISSN 0146-0412. https://doi.org/10.2514/3.47988.
6. Haukur Elvar Hafsteinsson. Porous Media in OpenFOAM®. *Chalmers University of Technology. Thecnical Report*, 2009.
7. W. X. M. Koh and E. Y. K. Ng. A CFD study on the performance of a tidal turbine under various flow and blockage conditions. *Renewable Energy. vol. 107, pp. 124–137*, 2017.
8. Dietrich Küchemann and Johanna Weber. *Aerodynamics of Propulsion*. McGraw-Hill, 1953.
9. C J Lawn. Optimization of the power output from ducted. In *Proceedings of the Institution of Mechanical Engineers–Part A– Power & Energy*, volume 217, pages 107–118, 2003.
10. Yuji Ohya, Takashi Karasudani, Akira Sakurai, Ken Ichi Abe, and Masahiro Inoue. Development of a shrouded wind turbine with a flanged diffuser. *Journal of Wind Engineering and Industrial Aerodynamics*, 96(5): 524–539, 2008. ISSN 01676105. https://doi.org/10.1016/j.jweia.2008.01.006.
11. M. Shives and C. Crawford. Developing an empirical model for ducted tidal turbine performance using numerical simulation results. *Proceedings of the Institution of Mechanical Engineers, Part A: Journal of Power and Energy*, 226(1): 112–125, 2012. ISSN 0957-6509. https://doi.org/10.1177/0957650911417958.
12. Felix Sorribes-Palmer, Angel Sanz Andres, Antonio Figueroa, Lorenzo Donisi, Sebastian Franchini, and Mikel Ogueta. Aerodynamic Design of a Wind Turbine Diffuser with Openfoam®. In *7th European-African Conference on Wind Engineering*, Liege, 2017.